Available online at www.sciencedirect.com
ScienceDirect
Trans. Nonferrous Met. Soc. China 32(2022) 251−261
Transactions of Nonferrous Metals Society of China
www.tnmsc.cn

# $Al_x$/HKUST-1 prepared by synthetic exchange as catalyst for reduction of NO by CO at low temperature

Li ZHANG[1,2], Jia-xiang ZHENG[2], Chao ZHANG[2], Yu-si WANG[2], Jing ZENG[2], Han-bing HE[2,3,4], Tie-chui YUAN[1], Yi-hong QIN[2], Ya-jie ZHENG[2]

1. Powder Metallurgy Research Institute, Central South University, Changsha 410083, China;
2. School of Metallurgy and Environment, Central South University, Changsha 410083, China;
3. State Environmental Protection Key Laboratory of Mineral Metallurgical Resources Utilization and Pollution Control, Wuhan University of Science and Technology, Wuhan 430081, China;
4. Key Laboratory of Metallurgical Emission Reduction & Resources Recycling (Ministry of Education), Anhui University of Technology, Ma'anshan 243002, China

Received 26 September 2020; accepted 18 November 2021

**Abstract:** $Al_x$/HKUST-1($x$=1/24, 1/12, 1/6, 1/3), one of the bimetallic copper-based organic framework materials, was successfully prepared by the synthetic exchange method and characterized by X-ray diffraction (XRD), scanning electron microscopy (SEM), specific surface area (BET), thermogravimetric analysis (TG), infrared spectra (IR), X-ray photoelectron spectroscopy (XPS), and $H_2$-temperature programmed reduction ($H_2$-TPR). The findings indicated that $Al_x$/HKUST-1 maintained the octahedral morphology of its precursor (HKUST-1). The thermal stability and catalytic reduction ability of HKUST-1 skeleton were improved by doping aluminum ($Al^{3+}$). $Al_{1/12}$/HKUST-1 showed the best performance among all samples, with a nitric oxide (NO) conversion rate of 100% at 210 °C (50 °C lower than that of HKUST-1). The valence kind of Al, Cu, and O in $Al_{1/12}$/HKUST-1 did not change after the catalytic reaction, but the contents of Al, Cu, and O in different forms changed significantly. The catalytic process of the $Al_x$/HKUST-1 followed a Langmuir−Hinshelwood mechanism.

**Key words:** copper-based organic framework; aluminium doping; synthetic exchange; denitration at low temperature; carbon monoxide

## 1 Introduction

The emission of nitrogen oxides ($NO_x$), including NO and $NO_2$, is harmful to the environment and human health, causing photochemical smog, acid rain, ozone depletion, and the greenhouse effect [1−3]. The selective catalytic reduction (SCR) of NO has been considered to be a promising solution to reduce NO pollution [1]. As one of the contaminants in exhaust, carbon monoxide (CO) is a promising reductant in SCR processes, and CO-SCR can reduce CO and $NO_x$ emissions at the same time to achieve the purpose of "using waste to treat waste" [3,4]. However, existing catalysts have many disadvantages, such as poor performance at low temperature, toxicity, and a narrow window of activated temperatures. At present, developing new types of catalysts which are non-toxic, harmless, stable in structure, and with superior low-temperature performance is extremely urgent.

Metal-organic frameworks (MOFs), a new class of crystalline materials formed by metal ions (joint) and organic ligands (linker) [5,6], have attracted much attention due to their varied nano-

**Corresponding author:** Han-bing HE, Tel: +86-13875985605, E-mail: hehanbinghhb@163.com
DOI: 10.1016/S1003-6326(21)65791-6

structures which can be controlled by a self-assembly process [7,8]. MOFs have been applied in the field of gas separation and storage [9], carbon-dioxide ($CO_2$) capture [10], sensing [11], drug delivery [12] and catalysis [13,14] based on their high pore volume and large specific surface [15−19].

The copper-based organic framework (i.e. $Cu_3(BTC)_2$, BTC=1,3,5-benzenetricarboxylate), named HKUST-1, is a representative MOF material with a microporous structure and open $Cu^{2+}$ sites with unsaturated coordination, in which the length of Cu—Cu is 2.628(2) Å, the length of Cu—OCO is 1.952(3) Å, and that of Cu—$OH_2$ is 2.165(8) Å [20]. HKUST-1, synthesized by CHUI et al [21], has a pocked-channel structure with specific surface area of 692.2 $m^2/g$, high thermal stability, small pore size (9 Å × 9 Å) and coordinatively unsaturated $Cu^{2+}$ sites [22]. DHAKSHINAMOORTHY et al [23] reported that HKUST-1 can be used to catalyze the oxidative hydroxylation of arylboronic acids to the corresponding phenols with a conversion rate of 80%. SHI et al [24] prepared new Cu-based MOFs by a solvothermal method and used them to catalyze the epoxidation reaction of olefins. Their findings showed that there was a high epoxide productivity of olefins and the Cu-MOF material maintained its structural integrity after the catalytic reaction.

However, the poor water and thermal stability of HKUST-1 [19] has hindered its large-scale application. Numerous methods have been reported to improve the thermal stability of HKUST-1. One simple and effective method is to form a bimetallic copper-based organic framework by doping with another metal element [1,4]. Usually, the post-synthetic ion exchange method [1,4] is used to produce a bimetallic copper-based organic skeleton, but the process is long and the number of exchange ions is difficult to control. In this study, a series of $Al_x$/HKUST-1($x$=1/24, 1/12, 1/6, 1/3), where $x$ represents the molar ratio of aluminum to copper in HKUST-1, were prepared by the synthetic exchange solvothermal method. The effect of Al content on the properties of HKUST-1 composites was studied. CO+NO reaction curves of $Al_x$/HKUST-1, carried out at temperatures lower than 300 °C, were obtained to illustrate the denitration mechanism of the HKUST-1 composites.

## 2 Experimental

### 2.1 Preparation of HKUST-1

HKUST-1 was prepared by the synthetic exchange solvothermal method. Briefly, 8 mmol of benzebe-1,3,5-tricarboxylic acid ($H_3BTC$, 98 wt.%) was dissolved in 40 mL of ethyl alcohol ($CH_3CH_2OH$, 99 vol.%) to obtain Solution A. Then, 12 mmol of copper nitrate trihydrate ($Cu(NO_3)_2$, 99 wt.%) was dissolved in 40 mL of ultra-pure water to obtain Solution B. Afterward, Solution A and Solution B were mixed together and stirred for 30 min. The mixed solution was transferred to a 100 mL stainless steel reactor with a polytetrafluoroethylene liner. The reactor was then placed in an oven at 120 °C for 24 h. The precipitated crystals from the solution were filtered and purified through ethyl alcohol and ultrapure water, repeatedly, to remove unreacted chemicals. Finally, the product was dried at 100 °C for 10 h before testing.

### 2.2 Synthesis of $Al_x$/HKUST-1($x$=1/24, 1/12, 1/6, 1/3)

Al doping in HKUST-1 was carried out by the ion exchange method, and the preparation steps were similar to those of HKUST-1. In the first step, 12 mmol of copper nitrate trihydrate ($Cu(NO_3)_2$, 99 wt.%) and a calculated amount of aluminum nitrate nonahydrate ($Al(NO_3)_3$, 99 wt.%) were dissolved in 40 mL of ultra-pure water to obtain Solution B. The following steps were the same as those in Section 2.1. After that, $Al_x$/HKUST-1 was prepared.

### 2.3 Characterization of catalysts

X-ray diffraction (XRD) data were collected on a Rigaku D/Max 2200 diffractometer employing Cu $K_\alpha$ radiation. Scanning electron microscopy (SEM) images were taken on a JEOL 3600 electron microscope using a 20 kV energy source under vacuum. The surface area of the catalysts was obtained by analyzing a nitrogen adsorption and desorption isotherm using the Brunauer-Emmett-Teller (BET) method on an ASAP 2020 HD88 (Micromeritics Instrument Corporation). The thermogravimetric analysis (TG) data were measured by a Q600 SDT instrument (America TA Instruments). The catalysts were degassed at 120 °C

for 8 h and analyzed with $N_2$ at 77 K. Infrared spectra (IR) data were recorded using a NICOLET 6700 (Thermo Scientific company). X-ray photoelectron spectrum (XPS) was acquired on a VG ESCALAB5 electron spectrometer equipped with a Mg $K_\alpha$ radiation source ($h\nu$=123.6 eV). The main C 1s peak (Binding energy=284.6 eV) was chosen as an internal standard to calibrate the energy scale. $H_2$-temperature programmed reduction ($H_2$-TPR) was carried out on a PCA−1200 chemisorption analyzer (BUILDER, Beijing, China).

### 2.4 Activity testing of catalysts

The experimental system consisted of three parts: gas distribution, catalysis and detection. NO was the main target for removal by denitration. The NO reduction reaction in specific stream was carried out with a flow reactor. For each experiment, 0.5 g of catalyst was placed in the center of a high-temperature resistant quartz glass tube with an inner diameter of 12 mm and a length of 500 mm. Then, the quartz glass tube with catalyst was placed in a tube electrical furnace with automatic temperature control. A gas mixture of CO and NO at a 1:1 molar ratio was filled into the reactor as a reactant at a constant space velocity of 24000 mL/(h·g). The real-time flue gas composition was recorded every minute by an online flue gas analyzer (MRU VARIO-plus), and an NDIR infrared sensor was used in the flue gas analyzer to detect the NO emission. When analyzing the data recorded by the flue gas analyzer per minute, the maximum deviation value was discarded and the average value was regarded as the gas composition at the corresponding temperature. The NO conversion ($X_{NO}$) was calculated as

$$X_{NO}=\{([NO]_{in}-[NO_x]_{out})/[NO]_{in}\}\times100\% \quad (1)$$

where $[NO]_{in}$ represents the NO content entering the quartz tube and $[NO_x]_{out}$ represents the contents of NO and $NO_2$ after the reaction, as recorded by the flue gas analyzer.

## 3 Results and discussion

### 3.1 XRD results of catalysts

The XRD results of HKUST-1 and $Al_x$/HKUST-1 are shown in Fig. 1. It was obvious that the curves of HKUST-1 and $Al_x$/HKUST-1 samples exhibited similar main characteristic peaks with the standard curve of HKUST-1, which confirmed that the synthetic samples maintained the structure of HKUST-1. The doping of Al weakened the diffraction peak intensity of HKUST-1. The crystal strength of HKUST-1 decreased with the increase of Al content, forming HKUST-1 with low crystallinity. The characteristic peaks at 5.7° and 11.7° remained essentially unchanged when $x$ increased from 1/24 to 1/12, while the peaks became weak and ultimately disappeared as $x$ increased from 1/12 to 1/3.

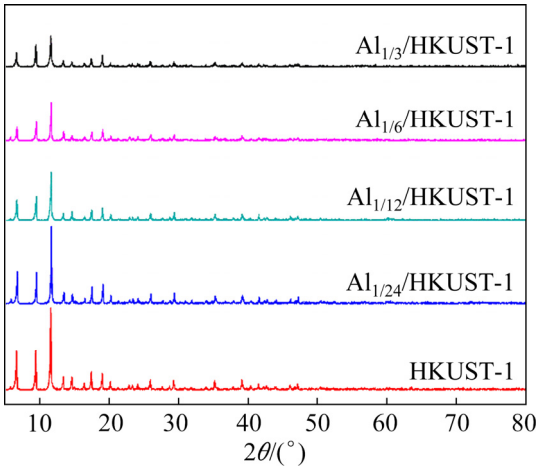


**Fig. 1** XRD patterns of HKUST-1 and $Al_x$/HKUST-1

### 3.2 SEM results of catalysts

SEM images of HKUST-1 and $Al_x$/HKUST-1 were observed, as shown in Fig. 2. The four samples maintained the morphology of a standard octahedral structure (Fig. 2). As the content of Al increased, metal oxides formed on the surface of the catalyst, and some damaged octahedrons appeared in the HKUST-1 structure. This indicates that the stability of the HKUST-1 structure can be compromised after a large number of Al ions enter the HKUST-1 structure.

### 3.3 BET results of catalysts

The specific surface areas of HKUST-1 and $Al_x$/HKUST-1 were investigated and the results are presented in Table 1. According to our analysis, both HKUST-1 and $Al_x$/HKUST-1 displayed a larger specific surface area than oxide catalysts of denitration, such as metal composite oxides and perovskite-type oxides. As the Al content of the catalyst increased, the specific surface area of $Al_x$/HKUST-1 continuously decreased. As observed in the SEM images (Fig. 2), the morphologies of the

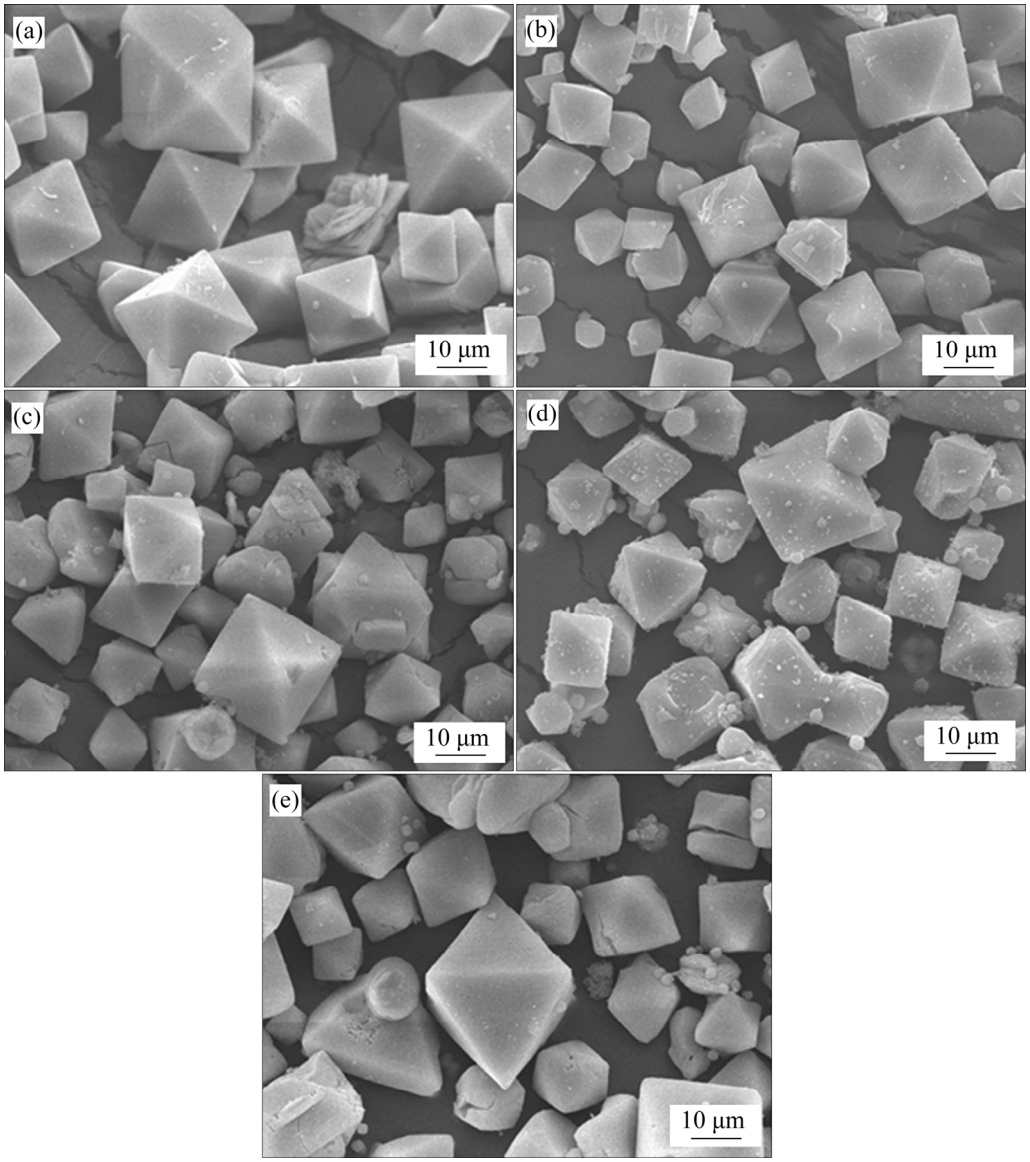


**Fig. 2** SEM images of HKUST-1 (a), $Al_{1/24}$/HKUST-1 (b), $Al_{1/12}$/HKUST-1 (c), $Al_{1/6}$/HKUST-1 (d) and $Al_{1/3}$/HKUST-1 (e)

**Table 1** Specific surface areas of HKUST-1 and $Al_x$/HKUST-1

| Sample | Special surface area/($m^2 \cdot g^{-1}$) |
|---|---|
| HKUST-1 | 1214.14 |
| $Al_{1/24}$/HKUST-1 | 1201.86 |
| $Al_{1/12}$/HKUST-1 | 1144.46 |
| $Al_{1/6}$/HKUST-1 | 1132.81 |
| $Al_{1/3}$/HKUST-1 | 987.90 |

samples were affected with the inclusion of Al, which might account for the gradual decrease in specific surface area. However, $Al_x$/HKUST-1 maintained a large specific surface area of around 1000 $m^2$/g. The large specific surface area of $Al_x$/HKUST-1 might provide a large adsorption interface for the gases involved in catalytic denitration reactions.

### 3.4 TG results of catalysts

The thermal stabilities of the synthetic samples were characterized by Q600 SDT and the results are shown in Fig. 3. The TG curves of all the samples exhibited a similar trend. With increasing temperatures from room temperature to 100 °C, the mass of the samples decreased markedly, corresponding to the loss of water adsorbed in the metal-organic framework. The mass of the samples decreased slowly between 100 and 200 °C, possibly due to the evaporation of crystalline water or oxidation combustion of some organic matter in the MOF. From 200 to 300 °C, the curves plateaued,

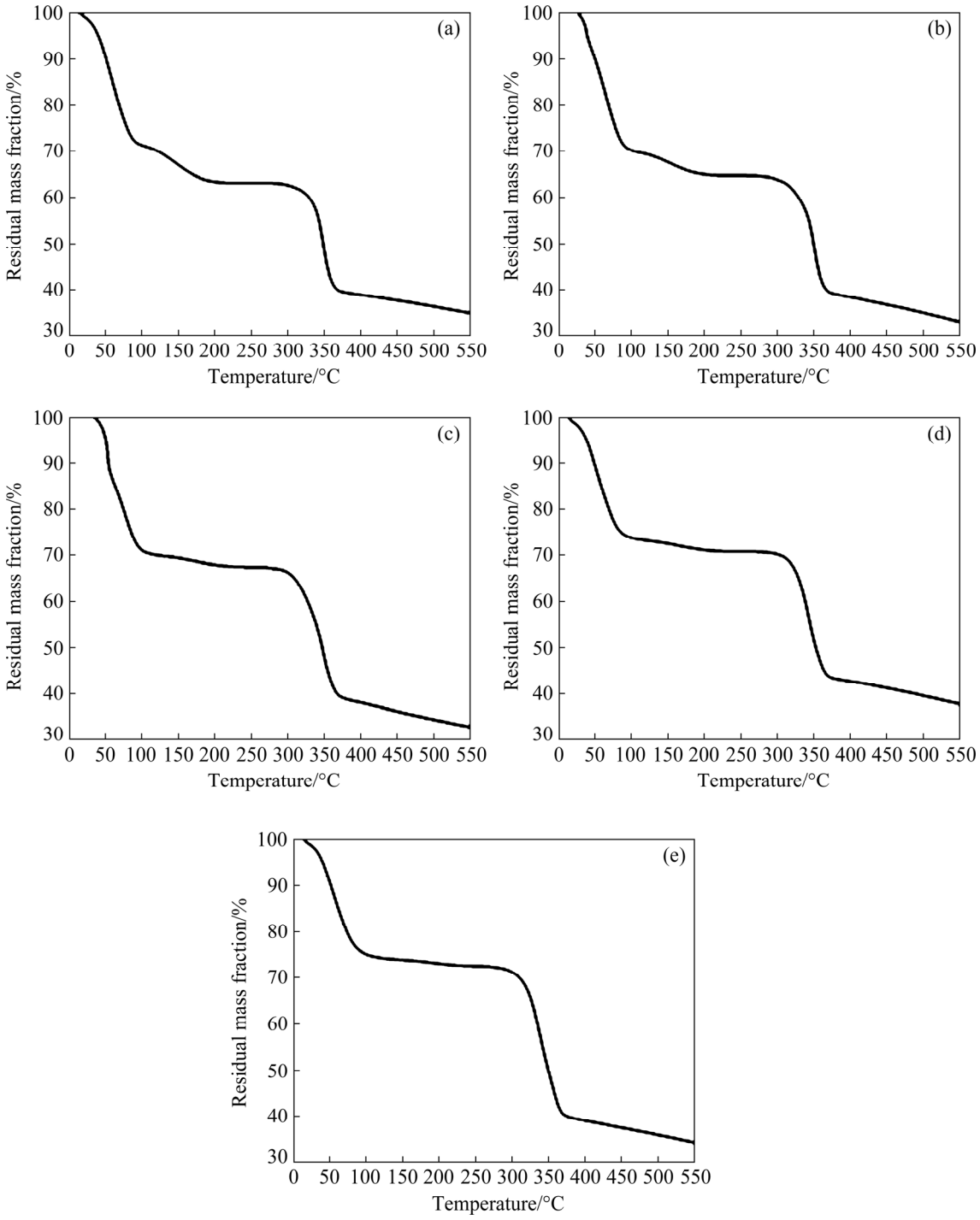


**Fig. 3** TG curves of HKUST-1 (a), $Al_{1/24}$/HKUST-1 (b), $Al_{1/12}$/HKUST-1 (c), $Al_{1/6}$/HKUST-1 (d) and $Al_{1/3}$/HKUST-1 (e)

indicating that the structure of the samples was stable in this temperature range. The mass of the samples decreased rapidly after 300 °C, likely due to the fact that such high temperatures resulted in the pyrolysis of the MOF. By comparing the value of the platform of HKUST-1 and $Al_x$/HKUST-1 before 300 °C, it was clear that HKUST-1 maintained about 60% of its original mass, while $Al_x$/HKUST-1 maintained more than 70%. Furthermore, there was a clear increase in the reserved mass of the samples with increased Al content, indicating that the addition of $Al^{3+}$ ion enhanced the thermal stability of HKUST-1.

### 3.5 IR results of catalysts

The infrared spectra of $H_3BTC$, HKUST-1 and $Al_x$/HKUST-1 are shown in Fig. 4. The IR spectrum of HKUST-1 showed the peak of Cu—O bond at

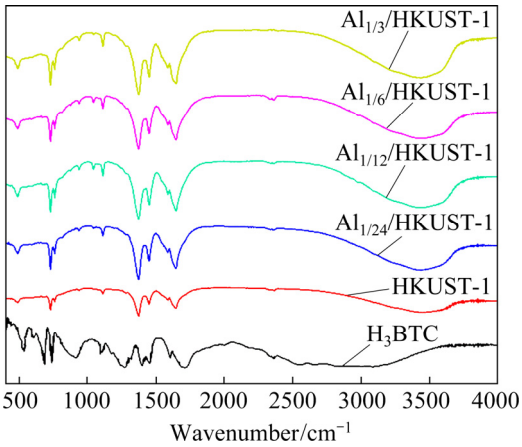


**Fig. 4** Infrared spectra of $H_3BTC$, HKUST-1 and $Al_x$/HKUST-1

500 cm$^{-1}$, which indicated that Cu atom was chelated or formed a bidentate ligand with $H_3BTC$ successfully. By comparing the curves of the $Al_x$/HKUST-1 samples with that of HKUST-1 in Fig. 4, it was evident that all the spectra showed similar characteristic peaks, demonstrating that the $Al_x$/HKUST-1 samples maintained the main structure of HKUST-1 [25]. Nevertheless, the peak corresponding to the Al—O bond at 1043 cm$^{-1}$ [26] appeared on the curves of $Al_x$/HKUST-1 samples, confirming that Al successfully entered the HKUST-1 structure and formed the $Al_x$/HKUST-1 structure.

### 3.6 XPS results of catalysts

The $Al_x$/HKUST-1 samples were further characterized by X-ray photoelectron spectroscopy (XPS) to identify the oxidation states of the metal compounds. The Al 2p, Cu 2p, and O 1s data of the $Al_x$/HKUST-1 samples are displayed in Fig. 5. Al kept its original valence state of +3 in nitrates and the spectra of Al 2p (Fig. 5(a)) can be divided into two sub-bands. The lower binding energy peak at 74.3 eV was assigned to $Al_2O_3$, and the higher binding energy peak (near 77.4 eV) probably originated from the Al—O bond related to atoms situated in sites adjacent to metal cation vacancies [27−29]. It indicated that all $Al^{3+}$ should be located at the metal nodes ($Al^{3+}$—$Al^{3+}$ and $Al^{3+}$—$Cu^{2+}$ paddlewheels). The deconvolution of the Cu 2p (Fig. 5(b)) revealed the existence of $Cu^+$ [30−32] with a peak binding energy around 932.4 eV and $Cu^{2+}$ [30−32] with peaks at 934.7, 940, and 944.6 eV both in HKUST-1 and

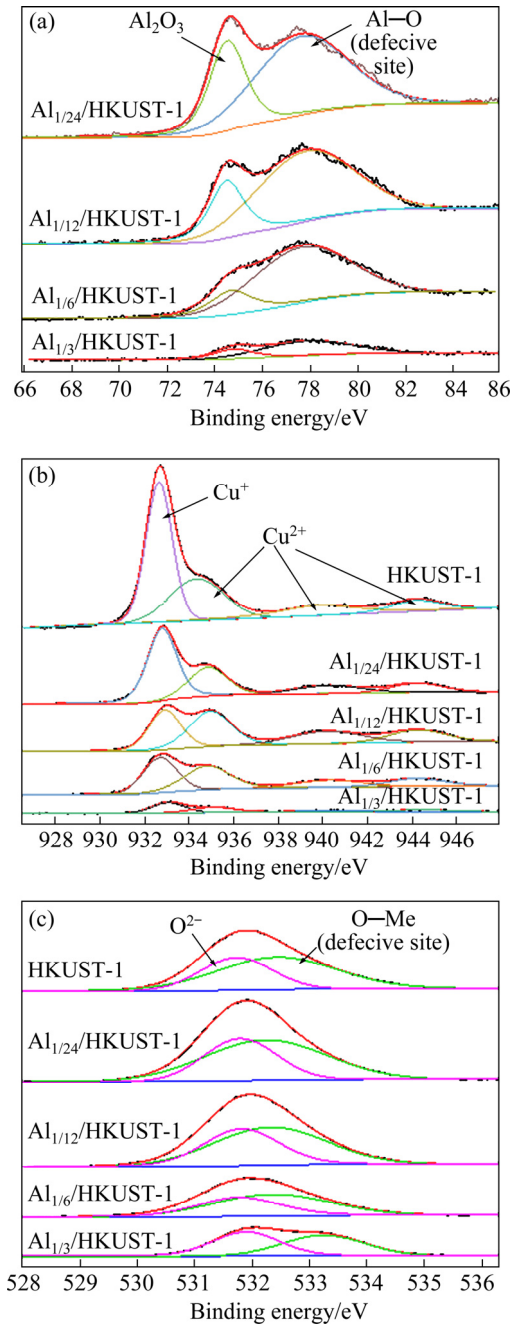


**Fig. 5** XPS spectra of HKUST-1 and $Al_x$/HKUST-1: (a) Al 2p; (b) Cu 2p; (c) O 1s

$Al_x$/HKUST-1 samples. These results provided solid evidence that both $Cu^{2+}$/$Cu^{2+}$ paddle-wheel units and $Cu^+$/$Cu^{2+}$ paddle-wheel defect pairs existed in HKUST-1 and $Al_x$/HKUST-1. The $Cu^+$/$Cu^{2+}$ paddle-wheel defects might be created by the thermal treatment during the preparation process. According to Fig. 5(c), the oxygen atoms existed in the two different chemical environments: one is the oxygen atoms in the oxide lattice ($O^{2-}$) with the peak at binding energy around 532 eV, and the other is the

oxygen atoms near vacancy-type defects in the organic skeleton with the peak at binding energy around 533 eV [27−29].

The results of the quantitative analysis shown in Table 2 revealed that the doped Al mainly entered the skeleton of HKUST-1 to form Al—O bond in the defective site. As the content of Al into $Al_x$/HKUST-1 increased, the content of Al—O bond in the defective site increased. In addition, doping Al into Cu-based MOF reduced the molar ratio of $Cu^+$ to $Cu^{2+}$ when $x$ was small (e.g. $x$=1/24, 1/12). However, as $x$ in $Al_x$/HKUST-1 increased further to 1/6 or 1/3, there was a corresponding increase in the molar ratio of $Cu^+$ to $Cu^{2+}$. As expected, the content of oxygen vacancy increased slightly as the Al entered the organic skeleton to replace copper, which played a key role in improving the catalytic ability of $Al_x$/HKUST-1. $Al_{1/12}$/HKUST-1 showed the highest content of O—Me in the defective site and it may possess good catalytic acidity.

### 3.7 $H_2$-TPR results of catalysts

In $H_2$-TPR analysis, the position of reduction peak roughly reflects the temperature at which the catalyst starts to consume reductant, and the area of the reduction peak roughly reflects the capacity of the catalyst consuming reductant. The results of $H_2$-TPR analysis of HKUST-1 and $Al_x$/HKUST-1 are shown in Fig. 6. After Al was doped into HKUST-1, the position of the reduction peak shifted to a lower temperature, and the area of the reduction peak decreased slightly, suggesting that the doping of Al increased the reduction capacity of the catalyst. $Al_{1/12}$/HKUST-1 had the strongest catalytic reduction capacity and the lowest catalytic reduction temperature in all $Al_x$/HKUST-1 samples.

### 3.8 Catalytic activity results of catalysts

The CO+NO reduction reaction was investigated by passing reaction gases through a quartz tube with the $Al_x$/HKUST-1 catalyst in a tube furnace whose temperature was controlled precisely by programmed temperature-control equipment. The reaction temperature increased from 30 to 280 °C in 3.5 h. The composition of the mixed gas after the denitration reaction was recorded every minute by the online gas analytical device. The results (Fig. 7) showed that the NO conversion of HKUST-1 was higher than that of the $Al_x$/HKUST-1 samples ($x$=1/24, 1/12, 1/6, 1/3) at a temperature lower than 150 °C. Interestingly, the NO conversion of $Al_x$/HKUST-1 increased rapidly with increasing temperature. The temperature of all $Al_x$/HKUST-1 samples with 100% NO conversion was lower compared to that of HKUST-1 (260 °C). $Al_{1/12}$/HKUST-1 showed the best catalytic activity, with NO conversion of 100% occurring at 210 °C (50 °C lower than that of HKUST-1). These results were consistent with those of the $H_2$-TPR analysis, strengthening the argument that $Al_{1/12}$/HKUST-1 exhibited the best catalytic performance due to its enhanced catalytic reduction capacity.

### 3.9 Catalytic reaction process

In order to better understand the changes of $Al_x$/HKUST-1 catalyst after the CO+NO reduction reaction, $Al_{1/12}$/HKUST-1 was selected for XPS spectrum analysis before and after the CO+NO reduction reaction (Fig. 8). It was obvious that the valence kind of Al, Cu, and O did not take any change after the catalytic reaction. The deconvolution of Al 2p (Fig. 8(a)) revealed that doped Al existed in the form of $Al_2O_3$ and Al—O bond in the defective site [27−29]. The Cu 2p spectra (Fig. 8(b)) revealed the existence of $Cu^+$ and $Cu^{2+}$ [30−32]. There were two forms of oxygen atoms (Fig. 8(c)), oxide lattice ($O^{2-}$) and oxygen atoms near the vacancy-type defects [27−29].

**Table 2** Analysis of valence state of Al, Cu, and O in HKUST-1 and $Al_x$/HKUST-1

| Sample | Molar fraction/% | | | | | |
|---|---|---|---|---|---|---|
| | $Al_2O_3$ | Al—O (defective site) | $Cu^+$ | $Cu^{2+}$ | $O^{2-}$ | O—Me (defective site) |
| HKUST-1 | − | − | 39.88 | 60.12 | 51.37 | 48.63 |
| $Al_{1/24}$/HKUST-1 | 41.49 | 58.51 | 36.48 | 63.52 | 43.03 | 56.97 |
| $Al_{1/12}$/HKUST-1 | 25.85 | 74.15 | 26.76 | 73.24 | 41.44 | 58.56 |
| $Al_{1/6}$/HKUST-1 | 26.61 | 73.39 | 42.14 | 57.86 | 44.37 | 55.63 |
| $Al_{1/3}$/HKUST-1 | 26.64 | 73.36 | 48.94 | 51.06 | 65.40 | 34.60 |

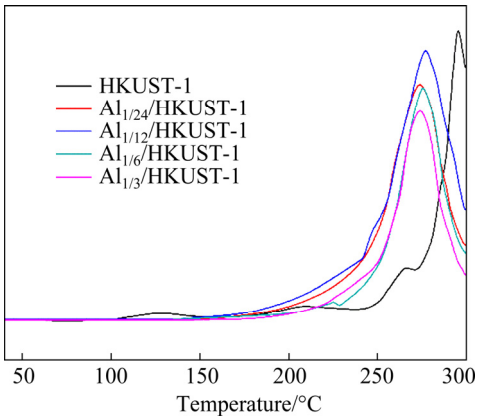


**Fig. 6** $H_2$-TPR curves of HKUST-1 and $Al_x$/HKUST-1

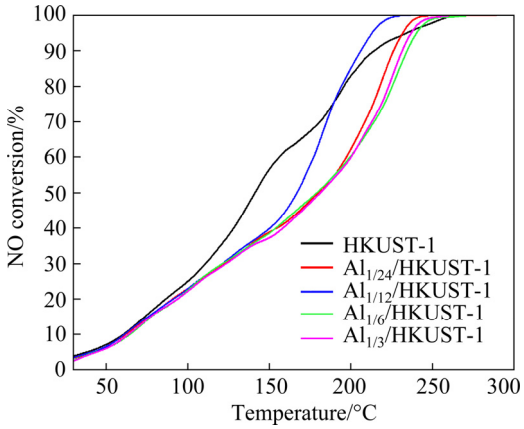


**Fig. 7** Catalytic activity curves of HKUST-1 and $Al_x$/HKUST-1

Although the valence kind of Al, Cu, and O kept the same before and after the CO+NO reaction, the contents of Al, Cu, and O in different forms changed significantly, as shown in Table 3. After the catalytic reaction, the content of the Al—O bond in the defective site, the content of $Cu^{2+}$, and the content of O — Me in the defective site decreased, while the content of $Al_2O_3$, the content of $Cu^+$, and the content of $O^{2-}$ increased, providing some basis for speculating the reaction process.

In addition, $Cu^+$ could absorb activated CO molecules to form $Cu^+(CO)_n$ ($n$=1−2) [25,30]. NO molecules are also absorbed by $Cu^+$ and form $Cu^+(NO)_n$ ($n$=1−2) [26]. $Al^{3+}$ entered the structure of HKUST-1 replaced Cu—O bond with Al—O bond, which formed plenty of oxygen vacancies to improve the catalytic process. Hence, this catalytic process followed a Langmuir−Hinshelwood mechanism. The mechanism of the catalytic reaction using $Al_x$/HKUST-1 as the catalyst are as follows:

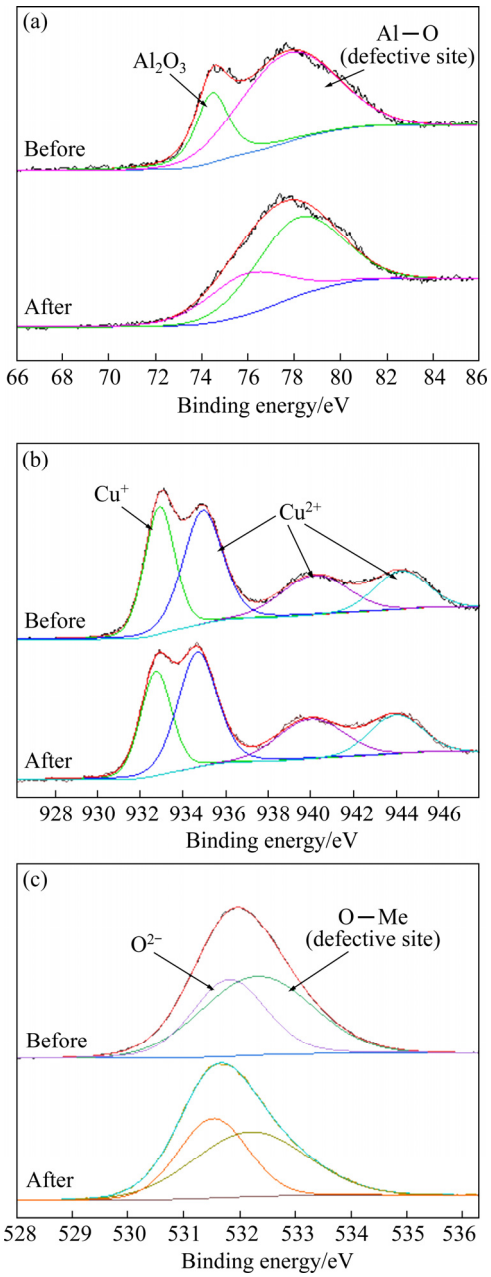


**Fig. 8** XPS spectra of $Al_{1/12}$/HKUST-1 before and after CO+NO reduction reaction: (a) Al 2p; (b) Cu 2p; (c) O 1s

$$CO(g)+Cu^+\rightarrow Cu^+CO(ad) \quad (2)$$

$$CO(g)+Cu^{2+}\rightarrow Cu^{2+}CO(ad) \quad (3)$$

$$CO(g)+Al^{3+}\rightarrow Al^{3+}CO(ad) \quad (4)$$

$$NO(g)+Cu^+\rightarrow Cu^+NO(ad) \quad (5)$$

$$Cu^+NO(ad)\rightarrow N(ad)+O(ad)+Cu^{2+} \quad (6)$$

$$Cu^+CO(ad)+O(ad)\rightarrow CO_2(g)+Cu^+ \quad (7)$$

$$Cu^{2+}CO(ad)+O(ad)\rightarrow CO_2(g)+Cu^{2+} \quad (8)$$

$$Al^{3+}CO(ad)+O(ad)\rightarrow CO_2(g)+Al^{3+} \quad (9)$$

$$N(ad)+N(ad)\rightarrow N_2(g) \quad (10)$$

**Table 3** Analysis of valence state of Al, Cu, and O in $Al_x$/HKUST-1

| Sample | Molar fraction/% | | | | | |
|---|---|---|---|---|---|---|
| | $Al_2O_3$ | Al—O (defective site) | $Cu^+$ | $Cu^{2+}$ | $O^{2-}$ | O—Me (defective site) |
| Before reaction | 25.85 | 74.15 | 26.76 | 73.24 | 41.44 | 58.56 |
| After reaction | 34.80 | 65.20 | 30.36 | 69.64 | 43.55 | 56.45 |

## 4 Conclusions

(1) The novel catalyst $Al_x$/HKUST-1 ($x$=1/24, 1/12, 1/6, 1/3) with obvious similarities in structure and octahedral morphology to HKUST-1, was successfully generated by the synthetic exchange solvothermal method.

(2) $Al^{3+}$ entered the structure of HKUST-1, and the Al—O bond replaced Cu—O bond. With the increase of Al content, the structure of HKUST-1 was damaged slightly, leading to the slight decrease of its specific surface area.

(3) Compared with HKUST-1, $Al_x$/HKUST-1 improved thermal stability and catalytic reduction ability, and $Al_{1/12}$/HKUST-1 exhibited the best properties in the CO+NO reduction reaction. $Al_{1/12}$/HKUST-1 had NO conversion of 100% at 210 °C, while HKUST-1 at 260 °C. Therefore, $Al_{1/12}$/HKUST-1 could be used as an effective catalyst for selective catalytic reduction of NO by CO at 210 °C.

(4) The valence kind of Al, Cu and O did not change after the catalytic reaction, but the contents of Al, Cu and O in different forms changed significantly. The catalytic process followed a Langmuir-Hinshelwood mechanism.

## Acknowledgments

The authors are grateful for the financial supports from the Natural Science Foundation of Hunan Province, China (No. 2020JJ4685), the Open Fund for Key Laboratory of Metallurgical Emission Reduction and Resources Utilization of Ministry of Education in Anhui University of Technology, China (No. JKF20-02), the Natural Science Foundation of Hunan Province, China (No. 2019JJ40378), the Open Fund for State Environmental Protection Key Laboratory of Mineral Metallurgical Resources Utilization and Pollution Control in Wuhan University of Science and Technology, China (No. HB201908), and the Scientific Technology Project of Strategic Emerging Industries and Major Achievement Transformation of Hunan Province, China (No. 2017GK4010). The authors thank AiMi Academic Services (www.aimieditor.com) for English language editing and review services.

## References

[1] QIN Yi-hong, HUANG Lei, ZHENG Jia-xiang, REN Qian. Low-temperature selective catalytic reduction of CO over A-Cu-BTC and $AO_x$/$CuO_y$/C catalyst [J]. Inorganic Chemistry Communications, 2016, 72: 78−82.

[2] LI Chun-yan, SHI Yong, ZHANG Hao, ZHAO Qi-dong, XUE Fang-hong, LI Xin-yong. Cu-BTC metal-organic framework as a novel catalyst for low temperature selective catalytic reduction (SCR) of NO by $NH_3$: Promotional effect of activation temperature [J]. Integrated Ferroelectrics, 2016, 172: 169−179.

[3] ZHANG Li, HUANG Lei, QIN Yi-hong, CHEN Bai-zhen. Structure and denitration performance of carbon-based catalysts prepared from Cu-BTC precursor [J]. Transactions of Nonferrous Metals Society of China, 2018, 28: 980−988.

[4] QIN Yi-hong, HUANG Lei, ZHANG Dang-long, SUN Li-guo. Mixed-node A-Cu-BTC and porous carbon based oxides derived from A-Cu-BTC as low temperature NO−CO catalyst [J]. Inorganic Chemistry Communications, 2016, 66: 64−68.

[5] SHERINO B, MOHAMAD S, ABDUL HALIM S N, ABDUL MANAN N S. Electrochemical detection of hydrogen peroxide on a new microporous Ni-metal organic framework material-carbon paste electrode [J]. Sensors and Actuators B: Chemical, 2018, 254: 1148−1156.

[6] YANG Hui-min, LIU Xian, SONG Xiu-li, YANG Tai-lai, LIANG Zhen-hai, FAN Cai-mei. In situ electrochemical synthesis of MOF-5 and its application in improving photocatalytic activity of BiOBr [J]. Transactions of Nonferrous Metals Society of China, 2015, 25(12): 3987−3994.

[7] TAN Zhi-dou, TAN Hai-yan, SHI Xin-yu, JI Zhuan, YAN Yun-fan, ZHOU Yin. Metal-organic framework MIL-53(Al)-supported copper catalyst for CO catalytic oxidation reaction [J]. Inorganic Chemistry Communications, 2015, 61: 128−131.

[8] HUANG Lei, YANG Zhi-hui, YAN LÜ-ji, ALHASSAN S I, GANG Hai-yin, WANG Ting, WANG Hai-ying. Preparation of 2D carbon ribbon/$Al_2O_3$ and nitrogen-doped carbon ribbon/$Al_2O_3$ by using MOFs as precursors for removing high-fluoride water [J]. Transactions of Nonferrous Metals Society of China, 2021, 31(7): 2174−2188.

[9] GONZÁLEZ-ZAMORA E, IBARRA I A. $CO_2$ capture under humid conditions in metal-organic frameworks [J]. Materials Chemistry Frontiers, 2017, 1(8): 1471−1484.

[10] PEREIRA DA SILVA G T, VEREGUE F R, MOISÉS M P, GUILHERME M R, RINALDI A W. Synthesis of $Al_2O_3$-nanowhisker-based HKUST-1 MOF composites[J]. Materials Chemistry and Physics, 2019, 232: 446−451.

[11] RAJKUMAR T, KUKKAR D, KIM K H, SOHN J R, DEEP A. Cyclodextrin-metal-organic framework (CD-MOF): From synthesis to applications [J]. Journal of Industrial and Engineering Chemistry, 2019, 72: 50−66.

[12] HU Ying-li, DAI Ling-mei, LIU De-hua, DU Wei, WANG Yu-jun. Progress & prospect of metal-organic frameworks (MOFs) for enzyme immobilization (enzyme/MOFs) [J]. Renewable and Sustainable Energy Reviews, 2018, 91: 793−801.

[13] HUANG Yuan-biao, LIANG Jun, WANG Xu-sheng, CAO Rong. Multifunctional metal-organic framework catalysts synergistic catalysis and tandem reactions [J]. Chemical Society Reviews, 2017, 46(1): 126−157.

[14] HU Mao-lin, SAFARIFARD V, DOUSTKHAH E, ROSTAMNIA S, MORSALI A, NOURUZI N, BEHESHTI S, AKHBARI K. Taking organic reactions over metal-organic frameworks as heterogeneous catalysis[J]. Microporous and Mesoporous Materials, 2018, 256: 111−127.

[15] SHERINO B, ABDUL HALIM S N, ABDUL MANAN N S, SARIP R, AL'ABRI A M, MOHAMAD S. Facile synthesis and characterization of novel dicarboxylate-Cu based MOFs materials [J]. Inorganica Chimica Acta, 2019, 491: 59−66.

[16] RANI R, DEEP A, MIZAIKOFF B, SINGH S. Enhanced hydrothermal stability of Cu MOF by post synthetic modification with amino acids [J]. Vacuum, 2019, 164: 449−457.

[17] WANG Rui, XU Hai-juan, ZHANG Ke, WEI Shi-yong, WU De-yong. High-quality Al@Fe-MOF prepared using Fe-MOF as a micro-reactor to improve adsorption performance for selenite [J]. Journal of Hazardous Materials, 2019, 364: 272−280.

[18] ZHONG Ming, KONG Ling-jun, LI Na, LIU Ying-ying, ZHU Jian, BU Xian-he. Synthesis of MOF-derived nanostructures and their applications as anodes in lithium and sodium ion batteries [J]. Coordination Chemistry Reviews, 2019, 388: 172−201.

[19] VAITSIS C, SOURKOUNI G, ARGIRUSIS C. Metal organic frameworks (MOFs) and ultrasound: A review [J]. Ultrasonics Sonochemistry, 2019, 52: 106−119.

[20] WANG Pei-fen, DU Xiao, CHEN Tian, HAO Xiao-gang, ABUDULA A, TANG Ke-yong, GUAN Guo-qing. A novel electroactive PPy/HKUST-1 composite film-coated electrode for the selective recovery of lithium ions with low concentrations in aqueous solutions [J]. Electrochimica Acta, 2019, 306: 35−44.

[21] CHUI S S Y, LO S M F, CHARMANT J P H, GUY ORPEN A, WILLIAMA I D. A chemically functionalizable nanoporous material $[Cu_3(TMA)_2(H_2O)_3]_n$ [J]. Science, 1999, 283:1148−1150.

[22] CHUI S S Y, LO S M F, CHARMANT J P H, ORPEN A G, WILLIAMS I D. Chemically functionalizable nanoporous material $[Cu_3(TMA)_2(H_2O)_3]_n$ [J]. Science, 1999, 283(5405): 1148−1150.

[23] DHAKSHINAMOORTHY A, ASIRI A M, GARCIA H. Mixed-metal or mixed-linker metal organic frameworks as heterogeneous catalysts [J]. Catalysis Science & Technology, 2016, 72: 2895−2899.

[24] SHI Da-bin, REN Yan-wei, JIANG Huan-feng, CAI Bo-wei, LU Jia-xian. Synthesis, structures, and properties of two three-dimensional metal-organic frameworks, based on concurrent ligand extension [J]. Inorganic Chemistry, 2012, 51: 6498−6506.

[25] TERENCIO T, RENZO F D, BERTHOMIEU D, TRENS P. Adsorption of acetone vapor by Cu-BTC: An experimental and computational study [J]. Journal of Physical Chemistry C, 2013, 117(49): 26156−26165.

[26] DING Shi-jin, WANG Peng-fei, ZHANG Wei, WANG Ji-tao, ZHANG Ye-wen, XIA Zhong-fu. Interaction between aluminum deposited by evaporation and Teflon AF film [J]. Acta Metallurgica Sinica, 2001, 37(3): 243−246. (in Chinese)

[27] FIGUEIREDO N M, CARVALHO N J M, CAVALEIRO A. An XPS study of Au alloyed Al−O sputtered coatings [J]. Applied Surface Science, 2011, 257: 5793−5798.

[28] BRAJPURIYA R, SHRIPATHI T. Investigation of Fe/Al interface as a function of annealing temperature using XPS [J]. Applied Surface Science, 2009, 255: 6149−6154.

[29] MENG Fan-ping, GE Fang-fang, CHEN Yu-yun, XU Gen-bao, HUANG Feng. Local structural changes induced by ion bombardment in magnetron sputtered ZnO: Al films: Raman, XPS, and XAS study [J]. Surface & Coatings Technology, 2019, 365: 2−9.

[30] GUO Peng-hu, FROESE C, FU Qi, CHEN Yen-ting, PENG Bao-xiang, KLEIST W, FISCHER R A, MUHLER M, WANG Yue-min. CuPd mixed-metal HKUST-1 as a catalyst for aerobic alcohol [J]. Journal of Physical Chemistry C, 2018, 122: 21433−21440.

[31] WANG Jun-jun, WANG Wei-jia, FAN Zhi-ying, CHEN Shuang, NEFEDOV A, HEIBLER S, FISCHER R A, WÖLL C, WANG Yue-min. Defect-engineered metal-organic frameworks: A thorough characterization of active sites using CO as a probe molecule [J]. Journal of Physical Chemistry C, 2021, 125: 593−601.

[32] WANG Wei-jia, SHARAPA D I, CHANDRESH A, NEFEDOV A, HEIBLER S, HEINKE L, STUDT F, WANG Yue-min, WÖLL C. Interplay of electronic and steric effects to yield low-temperature CO oxidation at metal single sites in defect-engineered HKUST-1 [J]. Angewandte Chemie International Edition, 2020, 59: 10514−10518.

# 合成交换法制备 $Al_x$/HKUST-1 催化 CO 低温还原 NO

张 丽[1,2]，郑佳翔[2]，张 超[2]，王于思[2]，曾 婧[2]，何汉兵[2,3,4]，袁铁锤[1]，秦毅红[2]，郑雅杰[2]

1. 中南大学 粉末冶金研究院，长沙 410083；
2. 中南大学 冶金与环境学院，长沙 410083；
3. 武汉科技大学 国家环境保护矿冶资源利用与污染控制重点实验室，武汉 430081；
4. 安徽科技大学 冶金减排与资源综合利用教育部重点实验室，马鞍山 243002

**摘 要**：采用合成交换法成功制备双金属铜基有机金属骨架材料 $Al_x$/HKUST-1($x$=1/24，1/12，1/6，1/3)，并采用 X 射线衍射(XRD)、扫描电子显微镜(SEM)、比表面积分析(BET)、热重分析(TG)、红外光谱(IR)、X 射线光电子能谱(XPS)以及 $H_2$ 程序升温还原($H_2$-TPR)技术对其进行表征。研究结果表明，$Al_x$/HKUST-1 维持前躯体(HKUST-1)的正八面体结构，掺铝($Al^{3+}$)后，HKUST-1 的热稳性和还原性能均得到提高。$Al_{1/12}$/HKUST-1 表现出最佳的催化活性，温度为 210 °C 时，催化脱硝率达到 100%，相比 HKUST-1 降低了 50 °C。催化反应后，$Al_{1/12}$/HKUST-1 中 Al、Cu 和 O 的价态种类没有发生改变，但是不同价态的 Al、Cu 和 O 的含量比值发生了明显变化。$Al_x$/HKUST-1 的催化过程遵循 Langmuir−Hinshelwood 反应机理。

**关键词**：铜基有机骨架；铝掺杂；合成交换法；低温脱硝；一氧化碳

**(Edited by Xiang-qun LI)**